nature photonics

LETTERS

PUBLISHED ONLINE: 27 MAY 2012 | DOI: 10.1038/NPHOTON.2012.112

Large spontaneous emission enhancement in plasmonic nanocavities

Kasey J. Russell*, Tsung-Li Liu, Shanying Cui and Evelyn L. Hu

Cavity–emitter coupling can enable a host of potential applications in quantum optics, from low-threshold lasers to brighter single-photon sources for quantum cryptography[1]. Although some of the first demonstrations of spontaneous emission modification occurred in metallic structures[2,3], it was only after the recent demonstration of cavity quantum electrodynamics effects in dielectric optical cavities[4] that metal-based optical cavities were considered for quantum optics applications[5–13]. Advantages of metal–optical cavities include their compatibility with a large variety of emitters and their broadband cavity spectra, which enable enhancement of spectrally broad emitters. Here, we demonstrate radiative emission rate enhancements approaching 1,000 for emitters coupled to the nanoscale gap between a silver nanowire and a silver substrate. A quantitative comparison of our results with analytical theory shows that the enhanced emission rate of gap-mode plasmons in our structures can yield high internal quantum efficiency despite the close proximity of metal surfaces.

In dielectric optical cavities, the signature of emission enhancement is unambiguous—changes in the radiative emission rate ν_R are correlated with proportional changes in the emission intensity. However, metal structures are inherently lossy and can suffer from high rates of non-radiative recombination (ν_{NR}). In addition, metallic structures can act as antennas to alter the efficiency of excitation and collection[14–16]. An ambiguous situation can therefore arise in which antenna effects increase the emission intensity while loss increases the total decay rate $\nu_T = \nu_R + \nu_{NR}$.

The experiments described here are designed to demonstrate unambiguously the large spontaneous emission enhancement capabilities of gap-mode plasmonic nanostructures. The enhancement we observe is significantly larger than that seen in dielectric cavities[17], but is comparable to the field enhancements in surface-enhanced Raman scattering from structures similar to the one reported here[18]. Our cavity design (Fig. 1) was based on surface plasmon coupling between a silver substrate and a silver nanowire lying parallel to the substrate[19]. This cavity geometry was chosen to enable a high degree of control over the spacing d_G between the nanowire and substrate, which was established by coating the substrate in thin uniform layers of Al_2O_3 and the fluorescent organic dye tris-(8-hydroxyquinoline) aluminium (Alq_3). This design ensures that the dye will be located at the high-field regions of the cavity modes (Fig. 1, inset). We fabricated six cavity structures with different gap spacings d_G ranging from ~5 to ~25 nm. These samples contained identical layers of Alq_3 (thickness, ~2.5 nm) but different thicknesses of Al_2O_3 spacer layer.

Fluorescence spectra from individual cavities show a strong modification from the uncoupled Alq_3 spectrum (Fig. 2a). The wavelengths of the peaks in the cavity spectra have been shown to correspond with the cavity resonances[19], establishing that cavity–emitter coupling can modify the spectral properties of the emission.

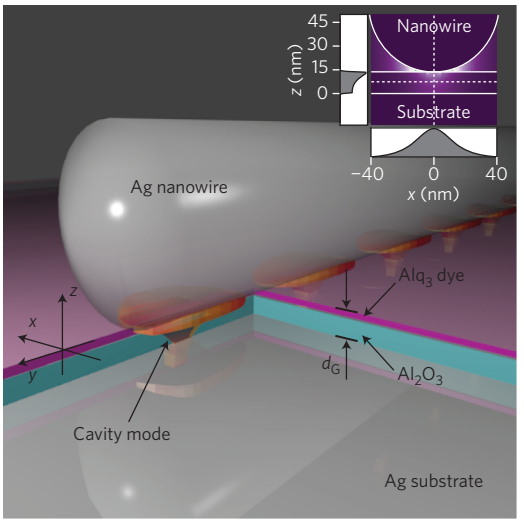

Figure 1 | Gap plasmon nanocavity containing coupled emitters. The cavity is composed of a silver nanowire and a silver substrate separated by a gap of thickness d_G set by a dielectric bilayer of Al_2O_3 and the fluorescent dye Alq_3. Inset: cross-section of a cavity showing strong confinement of the electric field within the gap. Plotted to the left and bottom are line cuts taken along the vertical and horizontal broken lines, respectively.

The dynamics of the fluorescence are also greatly modified by coupling to a cavity, with an enhancement of both decay rate and emission intensity (Fig. 2b). Fits indicate that the fluorescence decay is governed by a distribution of decay rates, which we interpret as different degrees of coupling to the cavity (Supplementary Fig. S1 and Section S1). Our analysis will focus on the fastest fitted decay rate (termed the total decay rate, ν_T) and its dependence on the thickness of the Al_2O_3 spacer layer. This ultimately yields a quantitative characterization of the emission enhancement characteristics of our structures.

Ideally, the incorporated dye absorbs energy from an incident laser pulse and then relaxes back to its ground state by coupling to the states of the cavity (referred to as 'gap modes'), leading to an enhanced radiative emission rate ν_R. However, there will also be coupling to the metal layers, which provides a non-radiative (lossy) pathway characterized by a non-radiative decay rate ν_{NR1}. Finally, intrinsic defects in the Alq_3 film itself lead to non-radiative decay with a characteristic rate ν_{NR2} (Supplementary Section S3). Both ν_{NR1} and ν_{NR2} contribute to $\nu_{NR} = \nu_{NR1} + \nu_{NR2}$, but in our case $\nu_{NR1} \gg \nu_{NR2}$ (Fig. 3), and we can therefore use the approximation $\nu_{NR} \approx \nu_{NR1}$ in our analysis. The important outcome of our experiment is that the relative influence of ν_R and ν_{NR} changes substantially with gap thickness. Analytical calculations indicate

Harvard University School of Engineering and Applied Sciences, 9 Oxford Street, McKay Laboratory, Cambridge, Massachusetts 02138, USA.
*e-mail: krussell@seas.harvard.edu

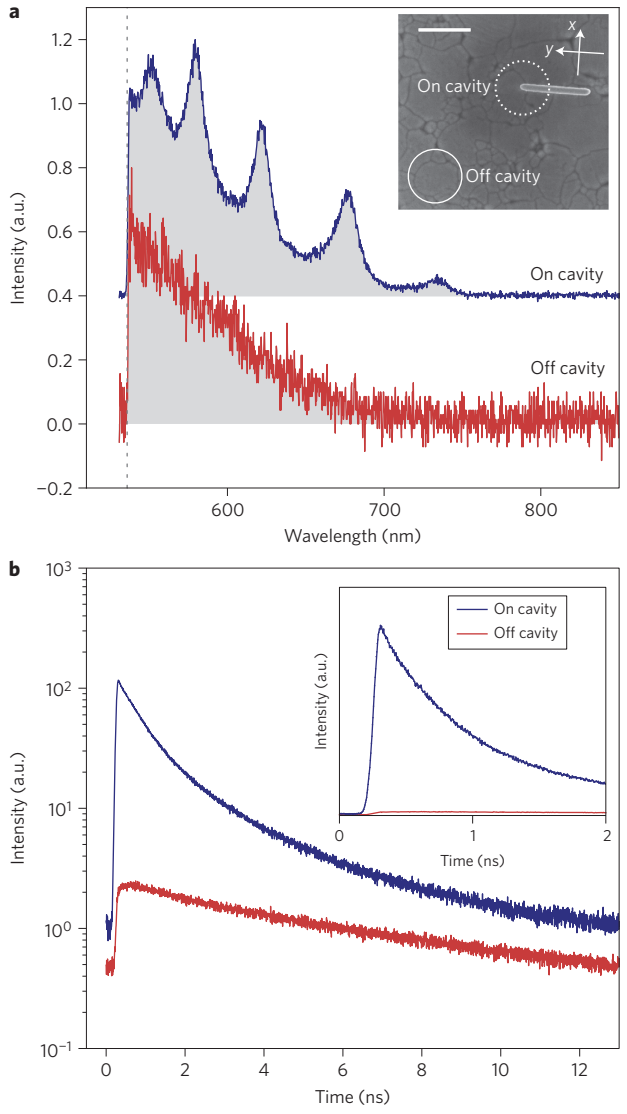

Figure 2 | Spectral and temporal characteristics of cavity-coupled Alq_3 fluorescence. a, Fluorescence spectra of Alq_3 on Al_2O_3/Ag with (on cavity) and without (off cavity) a silver nanowire. Wavelengths shorter than ~540 nm are blocked by a filter. Inset: SEM image of a cavity (scale bar, 500 nm) illustrating the location of the incident laser spot for on-cavity and off-cavity measurements. **b**, Time-resolved fluorescence measurements from the same samples as in **a**. Inset: detail of short time region on a linear intensity scale.

that for an electric dipole kept 2 nm from the top silver layer, the emission rate into the gap mode states ν_R is predicted to surpass the non-radiative decay rate ν_{NR} at a gap spacing of ~7 nm, resulting in an internal quantum efficiency greater than 0.5 (Fig. 3).

The calculations used to generate the results in Fig. 3 approximate the nanowire as a planar silver film (Supplementary Section S2). Owing to the close proximity of the nanowire to the Alq_3 layer, these calculations indicate that the non-radiative decay pathway ν_{NR} is ~250 times larger than the unperturbed spontaneous emission rate ν_R^0 of Alq_3 (that is, the radiative emission rate in a bulk dielectric film in the absence of metallic structures; Fig. 3a). Thus, at large spacer thicknesses where the gap plasmon emission rate ν_R is comparatively low, non-radiative decay dominates for these structures, resulting in quenching of the emission. As the spacer thickness is reduced, the increased confinement and emitter–mode overlap lead to enhanced emission into the gap-mode states. The rate of non-radiative recombination resulting from metal losses is not reduced (in fact, ν_{NR} increases as loss to the substrate becomes significant), yet the efficiency of gap plasmon emission increases dramatically as ν_R approaches and even exceeds ν_{NR}.

We can directly compare the results of the calculations for the total decay rate ν_T with the experimental data (with no fitting parameters) using only the experimentally determined radiative rate of Alq_3 in a bulk dielectric film, $\nu_R^0 \approx 1/46\ ns^{-1}$ (Fig. 4a, Supplementary Section S3). The planar model captures both the absolute scale of ν_T and its dependence on spacer thickness.

We may also indirectly probe the emission rate into the gap-mode states by correlating the peak intensity of the emission, a_0, with the total decay rate, ν_T. We note that for a decay $f(t) = a_0 \exp(-t\nu_T)$ characterized by the rate constant ν_T, the total number of photons emitted $N = \int_0^\infty f(t)dt = a_0/\nu_T$. N is also equal to the number of excited Alq_3 molecules N_0 times the collection efficiency η times the quantum efficiency $q = \nu_R/\nu_T$. We therefore find $N = qN_0\eta = N_0\eta\nu_R/\nu_T = a_0/\nu_T$, which simplifies to $N_0\eta\nu_R = a_0$.

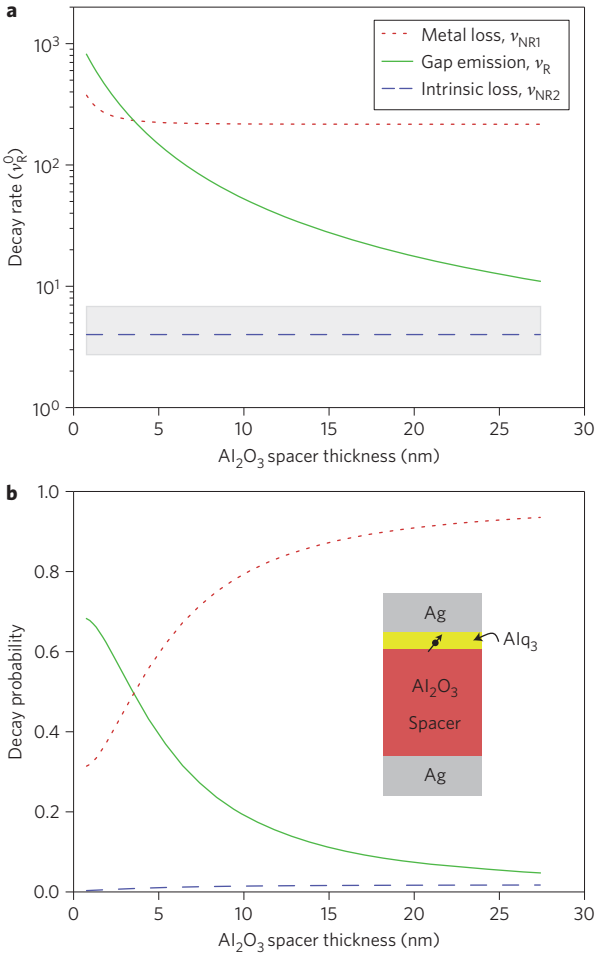

Figure 3 | Theoretical emission rate and efficiency versus spacer thickness for a silver gap structure. a, Decay rate via different available pathways versus Al_2O_3 spacer thickness for an electric dipole oscillating at 500 THz, 2 nm below the top metal layer, within a 2.6-nm-thick layer of Alq_3. Rates are normalized to the unperturbed decay rate of Alq_3 (ν_R^0). An isotropic distribution of dipole orientations is assumed, and the non-local dielectric response of the metal is included (Supplementary Section S2). The shaded band represents the 95% confidence interval of measured intrinsic non-radiative decay rates (Supplementary Section S3). **b**, Probability of decay via the different channels. Inset: schematic diagram of the planar structure used in the calculations.

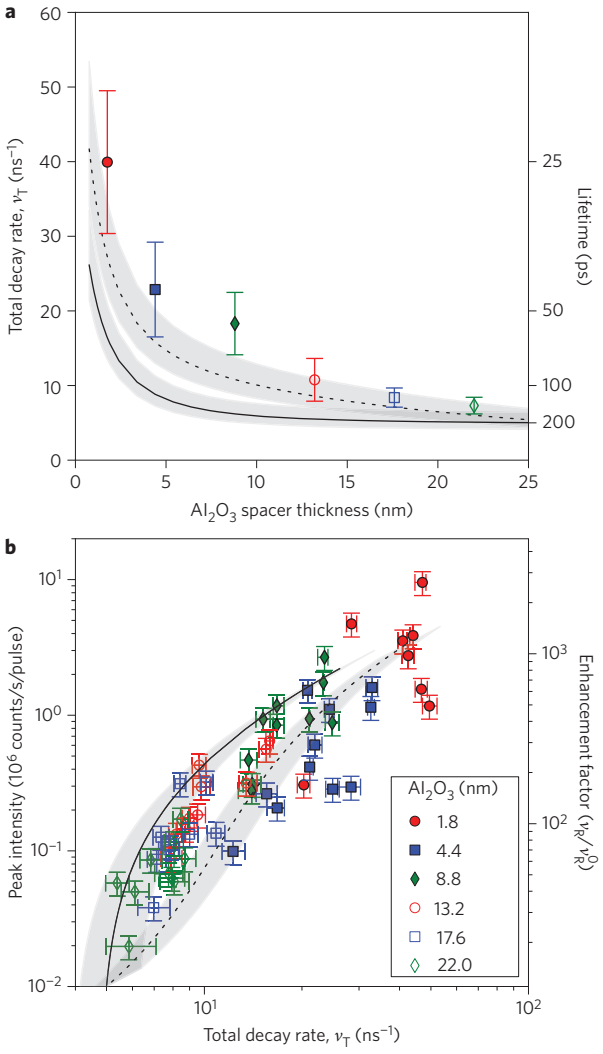

Figure 4 | Cavity enhancement characteristics. a, Total decay rate versus Al_2O_3 spacer thickness. Symbols and error bars represent means and standard deviations of measurements from all cavities on the sample, respectively. The solid line is predicted dependence (with no free parameters) from the calculation in Fig. 3 using the measured value of the bulk emission rate of Alq_3 ($\nu_R^0 \approx 1/46$ ns^{-1}, Supplementary Sections S2 and S3). The shaded band represents the 95% confidence interval of the measurement of ν_R^0. The broken line includes a small change in emitter–nanowire spacing, as suggested by numerical simulations (Supplementary Sections S2, S4). **b**, Peak intensity (a_0) versus total decay rate (ν_T) for all measured cavities. Points are experimental data and lines represent the same calculations as in **a**. Vertical scaling between lines and points is done with one fitting parameter, a proportionality constant ($a_C \approx$ 2,500 counts/s/pulse) relating the two vertical axes. The shaded band represents 95% confidence interval of the measurement of ν_R^0.

For constant collection and excitation efficiency, changes in the peak intensity a_0 can therefore be directly attributed to changes in ν_R. In fact, numerical simulations suggest that there are minor differences in excitation efficiency between samples, but that they are largely offset by changes in collection efficiency (Supplementary Section S4). To verify that the observed changes in ν_T are due primarily to changes in ν_R, we plot a_0 versus ν_T (Fig. 4b). We find that the peak intensity increases dramatically with total emission rate, confirming the presence of spontaneous emission enhancement into the gap modes. This dependence is in good agreement with that predicted by the calculation from Fig. 3, enabling a quantitative estimation of the magnitude of the emission enhancement (solid black line in Fig. 4b). The analytical calculation determines ν_R, which must be multiplied by a scaling factor (representing ηN_0) for comparison with the peak intensity a_0. The value used to give the agreement shown in Fig. 4b is of the same order of magnitude as that determined from analysis of off-cavity measurements, as predicted by simulations of the expected absorption (Supplementary Sections S3, S4). These data indicate that the emission enhancements achieved in our cavities approach 1,000 relative to the spontaneous emission rate of Alq_3 in a bulk dielectric film. As can be seen in Fig. 4b, the total decay rate of the brightest, fastest-decaying cavities is ~2,000 times larger than ν_R^0, but approximately half of that recombination is due to metal losses.

It should be noted that the analysis presented in Fig. 3 is for a planar metal–insulator–metal structure and therefore does not include the lateral confinement resulting from the finite length and width of the nanowire. Only recently have codes been developed that can calculate the electromagnetic response of arbitrary metallic shapes within a non-local treatment[20], and an accurate three-dimensional calculation is not currently possible. Nevertheless, we expect our analysis to capture the overall behaviour of our cavities because (i) the confinement in the direction perpendicular to the substrate is 10–100 times larger than the confinement in the lateral directions, and (ii) the spectral width of Alq_3 is much larger than the free spectral range of a cavity (Fig. 2a). The large spectral width of Alq_3 averages out the enhancement and suppression caused by the spectral confinement of the cavity, but it allows each emitter to couple to a multitude of cavity modes, ensuring spatial overlap with a subset of them. This interpretation is supported by the observed lack of dependence on nanowire length or diameter (Supplementary Fig. S4). These considerations suggest that even larger spontaneous emission enhancements can be achieved in the same structure for emitters that are spectrally and spatially matched with only one cavity mode.

We have therefore provided clear evidence that metal–optical nanocavities are capable of achieving a nearly 1,000-fold enhancement of spontaneous emission relative to the same emitter in a bulk dielectric film. The precise control afforded by our cavity design has enabled us to quantitatively characterize both the total decay rate and the emission intensity, ultimately yielding a detailed understanding of the relative contributions of emission enhancement and loss within our structure. Because gap structures such as the one described here are applicable to a wide variety of emitters, our results not only demonstrate large cavity quantum electrodynamics effects in a metal–optical structure, but also suggest a route to extend such effects to emitters that are incompatible either spectrally or structurally with conventional dielectric microcavity designs, including diamond nanocrystals, colloidal quantum dots and organic dyes.

Methods

Sample fabrication. Six samples were fabricated with different gap spacings d_G ranging from ~5 to ~25 nm. A silver substrate of subnanometre root-mean-square (r.m.s.) roughness (typically 0.5–0.8 nm r.m.s. over a 2 × 2 μm^2 area) was prepared by template-stripping from an atomically flat silicon wafer[21]. The thickness of the silver layer was ~300 nm, and it was anchored to a silicon 'handle' using epoxy (EPO-TEK 377, Epoxy Technologies), which was cured by baking the sample at 150 °C for ~3 h. Removal from the template was accomplished by sliding the blade of a razor under the corner of the silicon handle.

The freshly exposed, flat silver surface was immediately covered in Al_2O_3 using atomic layer deposition from precursors of trimethylaluminium and deionized water in a commercial reactor (Savannah, Cambridge Nanotech). The Al_2O_3 thickness was varied between samples to yield the desired d_G with fixed Alq_3 thickness.

The film of Alq_3 was thermally evaporated onto all samples simultaneously at a pressure of ~4×10^{-7} torr and rate of ~4.8 nm min^{-1} to a total thickness of ~2.6 nm, as measured with an *in situ* quartz crystal microbalance. After evaporation of Alq_3, the samples were stored in the dark in a vacuum dessicator when not being measured. Under these conditions, both the spectral and time-resolved fluorescence were found to be stable for at least several days.

Silver nanowires (Blue Nano) of diameter ~100 nm and length ~1–30 μm were deposited onto a piece of silicon in a droplet of ethanol that was allowed to dry. A piece of polydimethylsiloxane was pressed onto the surface of the silicon, removing some of the nanowires, some of which were then transferred to the $Alq_3/Al_2O_3/Ag$ structure via stamping.

Measurement procedure. Light from the pulsed, frequency-doubled beam ($\lambda \approx 460$ nm) of a Ti:sapphire laser was cleaned and approximately depolarized by coupling through a single-mode optical fibre, and then directed through a ×100, 0.9 NA microscope objective onto the sample in the direction normal to the substrate (along the *z*-axis). Fluorescence from the sample was collected through the same microscope objective, spectrally filtered to remove the laser signal, and spatially filtered to collect light only from the excitation region (that is, in a confocal microscopy arrangement) by coupling into a 10-μm-core multimode optical fibre. The signal was analysed using either a grating spectrometer with a liquid-nitrogen-cooled charge-coupled device camera (Princeton Instruments) or a fast avalanche photodiode with an impulse response with a full-width at half-maximum of ~50 ps (Micro Photon Devices). Spectra were typically acquired by integrating for 30 s, whereas time-resolved measurements were spectrally integrated and acquired for 2–5 min using time-correlated single photon counting.

All measurements were performed in a sample chamber continuously purged with nitrogen gas to reduce degradation of the Alq_3[22]. Measurements were performed at a laser power of ~40 nW, and multiple subsequent measurements of fluorescence lifetime yielded the same results.

Received 13 October 2011; accepted 17 April 2012; published online 27 May 2012

References

1. Noda, S., Fujita, M. & Asano, T. Spontaneous-emission control by photonic crystals and nanocavities. *Nature Photon.* **1,** 449–458 (2007).
2. Chance, R. R., Prock, A. & Silbey, R. Molecular fluorescence and energy transfer near interfaces. *Adv. Chem. Phys.* **37,** 1–65 (1978).
3. Moskovits, M. Surface-enhanced spectroscopy. *Rev. Mod. Phys.* **57,** 783–826 (1985).
4. Shields, A. J. Semiconductor quantum light sources. *Nature Photon.* **1,** 215–223 (2007).
5. Chang, D. E., Sorensen, A. S., Hemmer, P. R. & Lukin, M. D. Quantum optics with surface plasmons. *Phys. Rev. Lett.* **97,** 053002 (2006).
6. Maier, S. Effective mode volume of nanoscale plasmon cavities. *Opt. Quant. Electron.* **38,** 257–267 (2006).
7. Gong, Y. & Vučković, J. Design of plasmon cavities for solid-state cavity quantum electrodynamics applications. *Appl. Phys. Lett.* **90,** 033113 (2007).
8. Jun, Y. C., Kekatpure, R. D., White, J. S. & Brongersma, M. L. Nonresonant enhancement of spontaneous emission in metal–dielectric–metal plasmon waveguide structures. *Phys. Rev. B* **78,** 153111 (2008).
9. Esteban, R., Teperik, T. V. & Greffet, J. J. Optical patch antennas for single photon emission using surface plasmon resonances. *Phys. Rev. Lett.* **104,** 026802 (2010).
10. Vesseur, E. J. R., de Abajo, F. J. G. & Polman, A. Broadband Purcell enhancement in plasmonic ring cavities. *Phys. Rev. B* **82,** 165419 (2010).
11. Miyazaki, H. T. & Kurokawa, Y. Squeezing visible light waves into a 3-nm-thick and 55-nm-long plasmon cavity. *Phys. Rev. Lett.* **96,** 097401 (2006).
12. Gong, Y., Lu, J., Cheng, S.-L., Nishi, Y. & Vučković, J. Plasmonic enhancement of emission from Si-nanocrystals. *Appl. Phys. Lett.* **94,** 013106 (2009).
13. Jun, Y. C., Pala, R. & Brongersma, M. L. Strong modification of quantum dot spontaneous emission via gap plasmon coupling in metal nanoslits. *J. Phys. Chem. C* **114,** 7269–7273 (2010).
14. Brongersma, M. L. & Shalaev, V. M. The case for plasmonics. *Science* **328,** 440–441 (2010).
15. Schuller, J. A. *et al.* Plasmonics for extreme light concentration and manipulation. *Nature Mater.* **9,** 193–204 (2010).
16. Gramotnev, D. K. & Bozhevolnyi, S. I. Plasmonics beyond the diffraction limit. *Nature Photon.* **4,** 83–91 (2010).
17. Hennessy, K. *et al.* Quantum nature of a strongly coupled single quantum dot–cavity system. *Nature* **445,** 896–899 (2007).
18. Yoon, I. *et al.* Single nanowire on a film as an efficient SERS-active platform. *J. Am. Chem. Soc.* **131,** 758–762 (2009).
19. Russell, K. J. & Hu, E. L. Gap-mode plasmonic nanocavity. *Appl. Phys. Lett.* **97,** 163115 (2010).
20. McMahon, J. M., Gray, S. K. & Schatz, G. C. Nonlocal optical response of metal nanostructures with arbitrary shape. *Phys. Rev. Lett.* **103,** 097403 (2009).
21. Nagpal, P., Lindquist, N. C., Oh, S.-H. & Norris, D. J. Ultrasmooth patterned metals for plasmonics and metamaterials. *Science* **325,** 594–597 (2009).
22. Priestley, R., Sokolik, I., Walser, A. D., Tang, C. W. & Dorsinville, R. Photooxidation effects on picosecond photoluminescence and photoconductivity in tris-(8-hydroxyquinoline) aluminum (Alq3). *Synth. Met.* **84,** 915–916 (1997).

Acknowledgements

The authors acknowledge support from the NSF/NSEC (NSF/PHY-06-46094), the use of NSF/NNIN facilities at Harvard University's Center for Nanoscale Systems, and the use of the HPC computer cluster at Harvard.

Author contributions

K.J.R. designed and performed experiments, analysed data and wrote the paper. T.L.L. designed and performed experiments and analysed data. S.Y.C. performed experiments. E.L.H. designed experiments, analysed data and wrote the paper.

Additional information

The authors declare no competing financial interests. Supplementary information accompanies this paper at www.nature.com/naturephotonics. Reprints and permission information is available online at http://www.nature.com/reprints. Correspondence and requests for materials should be addressed to K.J.R.